Cell elongation via intrinsic antipodal stretching forces

T. Sawetzki, C. D. Eggleton, and D. W. M. Marr

Phys. Rev. E **86**, 061901 — Published 5 December 2012

DOI: 10.1103/PhysRevE.86.061901

The optical ravine – cell elongation via intrinsic antipodal stretching forces

T. Sawetzki[1], C.D. Eggleton[2], D.W.M. Marr[1]

[1] *Chemical and Biological Engineering Department, Colorado School of Mines, Golden, CO 80401*

[2] *Department of Mechanical Engineering, University of Maryland, Baltimore County, Baltimore, MD 21250*

PACS numbers: 87.16.dm, 87.15.La, 83.85.Ei, 87.80.Cc

To probe the mechanical properties of cells, we investigate a novel technique to perform deformability-based cytometry that inherently induces normal antipodal surface forces using a single line-shaped optical trap. We show theoretically that these opposing forces are generated simultaneously over curved microscopic object surfaces with optimal magnitude at low numerical apertures, allowing the directed stretching of elastic cells with a single, weakly-focused laser source. Matching these findings with concomitant experimental observations, we elongate red blood cells, effectively stretching them within the narrow confines of a steep, optically-induced potential well.

I. INTRODUCTION

Over the past few decades, focused laser beams, so-called optical tweezers, have successfully been employed to trap and manipulate small dielectric objects including micron-sized beads [1] and biological objects such as cells [2]. In this, momentum transferred at the particle surface via light refraction generates restoring forces directed

towards the laser focus, forces that can be used for strong localization of rigid microscopic objects. When trapping soft dielectric particles including living cells, however, these surface forces can induce deformation. As a result, optical tweezers provide an excellent method for the noncontact, damage-free probing of the elastic behavior of cells, a relevant measure as mechanical properties are often connected to their health and viability [3, 4]. Demonstrating this, point laser sources have been used to stretch red blood cells (RBCs) by manipulating attached colloidal particles [5, 6], by employing the light pressure of two counter-propagating beams [7, 8] and by applying other multiple-beam techniques [9-11]. However, due to the small effective stretching cross sections of point laser traps and the long time scales required for individual measurements, these methods have proven cumbersome and are best employed on single, localized cells at throughput rates of < 0.1 cell/s [12].

Because of cellular heterogeneity, the fields of microbiology and biophysics have become increasingly concerned with high-throughput individual-cell studies that are not subject to the averaging with bulk measurement approaches that mask small sub-populations. This need has motivated the field of flow cytometry and the development of instruments capable of measurement rates of > 1000 cells/s. These tools have proven indispensible for not only laboratory researchers but also the biomedical community in applications as common as measuring a complete blood count. This current disconnect of 4-5 orders of magnitude between standard high-throughput and single-cell stretching measurement capability defines the eventual goal of deformability-based cell cytometry. To move toward this, the applicability of laser diode bars as a tool for high flow rate

performance has been demonstrated both experimentally [13] and in simulations [14], with feasible throughputs only limited by trap dimensions and camera speed.

So far, however, and though we understand how forces arise, we lack a description of the underlying mechanisms responsible for cell deformation and with it the ability to optimize the approach. Here, and through modeling the anisotropic cell interactions, we demonstrate how a single, extended line-shaped trap inherently provides opposing forces and, as a result, is ideally suited for applications beyond single cell probing. To gather new insight into the origin of optically-induced cell deformation, we model the laser beam using experimentally measured parameters, which enables us to predict optical forces and subsequent deformation on our chosen model system, the red blood cell. These results both demonstrate the underlying principles of cell stretching and identify the most important system operation parameters for improving performance. In this, we observe that the intrinsic anisotropy of laser diode bars and the associated optical forces leads to axial elongation along the linear trap perpendicular to the incident alignment-free laser source, greatly simplifying both implementation and imaging. Based on these findings, we demonstrate how device performance can be optimized through the use of low numerical aperture (*NA*) optics, a result unique for optical tweezers approaches.

II. MODEL

Unlike conventional optical tweezers, the ravine-shaped potential landscape of our approach constricts the mobility of captured dielectric particles perpendicular to the trap while allowing translation along the line axis. As shown in Fig. 1, this particular

geometry can be generated with a single astigmatic source, whose beam axis in the *x*-direction is focused in the $z = 0$ plane while remaining extended along *y*. To determine the resulting distribution of forces exerted on a deformable cell surface, we perform simulations modeling the optical trap as a series of discrete rays using ray-tracing methods [13-16].

Assuming different Gaussian beam profiles along each beam axis, we model the astigmatic laser beam using the focusing angles $\alpha_{x/y}$ and the distance between the two foci d_f (Fig. 1). The *NA*s in the *x*- and *y*-directions are given by $NA_{x/y} = n \sin \alpha_{x/y}$, where n_W is the refractive index of water. Trap dimensions are defined by trap width w_0 and length l_0 in the imaged focal plane at $z = 0$:

$w_0 = \lambda / \pi \alpha_x$ and

$$l_0 = \left(\lambda / \pi \alpha_y\right)\left(1 + d_f^2 / z_{Ry}^2\right)^{1/2}, \qquad (1)$$

with laser wavelength λ and Rayleigh range in *y*, $z_{Ry} = l\left(d_f\right) \cdot \pi / \lambda$.

We model the optical trap at $z = 0$ as an array of discrete rays, set up in $2N$ and $2M$ steps of size Δx and Δy, spanning the width $-2w_0 \ldots +2w_0$ and length $-2l_0 \ldots +2l_0$. *N* and *M* are chosen to allow the cell to interact with 2000 x 2000 rays, realized by individual emitters of size less than 4 nm x 4 nm to provide a sufficiently fine mapping over a spherical RBC surface of radius $r = 3.5$ μm in the center of the laser focus. Each ray, with parameters *n* (*m*) ranging in value from $-N$ ($-M$) to $+N$ ($+M$), is weighted according to the Gaussian intensity distributions along both directions with $I_{nm} = I\left(n\Delta x, m\Delta y\right)$:

$$I_{nm} = \frac{P}{2\pi\Delta x\Delta y \cdot w_0 l_0} \exp\left[-\frac{1}{2}\left(\frac{(n\Delta x)^2}{w_0^2} + \frac{(m\Delta y)^2}{l_0^2}\right)\right]. \quad (2)$$

Consequently, each discrete ray transports a momentum $p_{nm} = p(n\Delta x, m\Delta y)$ per unit time t of

$$\frac{p_{nm}}{t} = n_W \frac{I_{nm} \cdot \Delta x\Delta y}{c}, \quad (3)$$

where c is the speed of light. The path of each incident ray vector $\vec{v}_{nm}^{(i)} = (x_n(z), y_m(z), z)$ with parameters (n,m) is defined by its components

$x_n(z) = n\Delta x\left(1 + z^2 / z_{Rx}^2\right)^{1/2}$ and

$$y_m(z) = m\Delta y\left[1 + \left(z - d_f\right)^2 / z_{Ry}^2\right]^{1/2}, \quad (4)$$

with Rayleigh ranges $z_{Rx/y}$ in x and y. We model the membrane of a spherical RBC composed of discrete surface elements ΔA using spherical coordinates (inclination θ and azimuth ϕ) with a cell refractive index n_{RBC} = 1.39 and cell center at the origin of the Cartesian coordinate system used for description of the beam. Using Eq. (4), we calculate the intersection of each light vector $\vec{v}_{nm}^{(i)}$ with the surface element $\Delta A(\theta,\phi)$ of the RBC membrane. Applying Snell's law on the local cell geometry, we determine the vectors of transmitted (refracted) and reflected light, $\vec{v}_{nm}^{(t)}$ and $\vec{v}_{nm}^{(r)}$. With orientation of the surface element $\Delta A(\theta,\phi)$ and the linear polarization of the laser light parallel to the line trap, we determine the local reflection and transmission coefficients $T_{\theta,\phi}$ and $R_{\theta,\phi}$ and obtain the normal force $\vec{f}_{nm}$ transferred to the surface element via a discrete ray with parameters n and m:

$$\vec{f}_{nm} = \frac{p_{nm}}{t}\left[\vec{v}_{nm}^{(i)} - \left(\frac{n_W}{n_{RBC}} T_{\theta,\phi}\vec{v}_{nm}^{(t)} + R_{\theta,\phi}\vec{v}_{nm}^{(r)}\right)\right]. \quad (5)$$

Following the path of each ray through the model cell to its exit point, we obtain the complete distribution of optical forces over the cell surface and the local photonic stress $\sigma(\theta,\phi)$ on a given surface element $\Delta A(\theta,\phi)$ by dividing by its area *a*.

III. RESULTS

Figure 2 shows the total calculated photonic stress distribution on the front- (a) and backside (c) of a spherical RBC in the imaged focal plane with the indicated trap axis. As all forces act normal to the surface, the dominant stress contribution responsible for elongation is located in membrane domains near $z = 0$. The opposing cell edges in *y* are located in the maximum intensity region of the focused beam. As a result, strong deformation forces arise along the linear trap. To provide sufficient stress anisotropy over the membrane for efficient directed elongation, beam width w_0 along *x* must be smaller than the cell diameter. Therefore, low laser intensity can be found in remote membrane regions perpendicular to the trap axis with resulting significantly lower optical forces along *x*. This fundamental anisotropy of laser light distribution over the cell strongly depends on the line width w_0 and therefore on NA_x of the beam. In contrast, the parameters NA_y and d_f have little influence on the stretching forces along *y*, as trap length l_0 must be considerably larger than the cell diameter.

The dependence of the photonic stress on the NA_x of the focused laser is shown in Fig. 2 along with illustrated beam paths. In this, the membrane area exposed to light clearly

depends on the optical focus. In the case of lower NA_x = 0.28 (Fig. 2 (a) and (c)), optical forces are distributed over a larger area, leading to lower photonic stress and a smaller influence on the membrane. For the larger NA_x = 0.39 (Fig. 2 (d) and (f)) the opposite is true as the incident light is focused on the backside of the cell. As a result, cells can be deformed with varying efficiency, depending on the overall anisotropy of generated forces.

Figure 3 further demonstrates the strong influence of NA_x on the resulting RBC membrane stress. The inset shows the monotonic increase of optical forces with NA_x due to higher focusing and therefore increasing intensity, while the membrane area over which these forces are applied exhibits a clear minimum. At NA_x smaller than the optimum, the area increases as a result of increasing beam width w_0; for larger NA_x the area expands due to increasing beam divergence φ_x. As a consequence of these competing effects, the generated membrane stress, and therefore the stretching efficiency, is maximized at a comparatively low value of $NA_x \approx 0.5$. Taking advantage of this unique result for an optical tweezers application, we experimentally test our theoretical model under ideal conditions for stretching cells at optimized applied optical powers.

IV. EXPERIMENTS

A conventional Gaussian laser beam can be used to realize a line-shaped optical trap through the astigmatism generated by cylindrical optics [17, 18]. To simplify optical design and implementation, however, we employ a single inexpensive laser diode bar [19-21] (JDS Uniphase-2472-P1, λ = 810 nm , 1.4 W max. power) whose active area of

1 µm x 200 µm emits an astigmatic laser beam (slow axis 12˚, fast axis 32˚ divergence). This light is expanded using a 20x Zeiss microscope objective and refocused into the sample with a 40x (Nikon, A-Plan 0.65) or 60x (Olympus, Plan Apo 1.45 Oil) microscope objective. As the astigmatic nature of the beam is preserved, we image the two perpendicular beam axes of the laser source at different focal distances, realizing a line-shaped optical trap (Fig. 1). Line length and width depend directly on the *NA*s of the imaging optical system for both beam axes. The use of a low-*NA* optical system limits optical trapping to two dimensions; however this does not prevent stretching in confined environments and provides significant advantage in both simplicity and application.

We directly measure the beam shape at different positions z using knife-edge methods and obtain width $w(z)$ and length $l(z)$ of the Gaussian intensity distributions along x and y. Here, the measured focusing angles $\alpha_{x/y}$ of the astigmatic beam are used to approximate the line width according to Eq. (1) while the line length l_0 is measured directly through image analysis. The employed 40x (60x) objectives create linear traps with Gaussian beam widths of 1.23 µm x 29.3 µm (0.87 µm x 19.6 µm) along x and y with $NA_x = 0.28$ (0.39) and a distance between the two focal planes of $d_f = 176$ µm (59 µm).

To compare to our theoretical data and validate our results, we use the well-studied system of human RBCs [22-24]. To provide sufficient dilution for single-cell experiments, a drop of blood, ~ 1.5 µl, was diluted in 500 µl buffer solution at 155 mOsm (1.25% sodium citrate, Sigma Aldrich) and 0.167% bovine serum albumin (BSA, Sigma Aldrich). RBCs were swollen to a nearly spherical shape to enhance detection and facilitate

comparison to modeling, increasing the membrane elastic modulus by a factor of ~2 [25]. Polydimethylsiloxane (PDMS) -based microfluidic devices were fabricated using common soft lithography methods [26], creating straight microfluidic channels with dimensions of 25 mm x 1000 μm x 10 μm. These were bonded to glass microscope slides and rinsed with BSA buffer solution for ~ 3 h prior to experiments to prevent cell adhesion to the channel walls.

We study individual RBCs captured within the linear trap in static environments, where samples were imaged using a high-speed camera system (EPIX silicone video 643M), recording at 1000 fps. Custom-made image detection software was used to fit ellipses to the outlines of imaged RBCs, obtaining sub-pixel resolution for the long and short axes at a noise level of ± 15 nm for single image analysis. We reduce absolute errors by averaging up to 100 individual images, easily accessible in the timescales associated with the high-speed camera. We employ laser powers up to 700 mW, where the power is distributed over the length of the trap leading to a total of less than 75 mW per cell at the upper operation limit. Such low local intensities avoid cell damage and minimize any potential negative impact on cell viability [2].

We predict cell deformation based on the calculated distribution of optical forces and the cell elastic modulus E where the external loading on a cell surface element is balanced by the inner-membrane tensions N_1 and N_2. Here, the radial force N_2 around an elementary ring of the membrane at inclination θ is estimated with the total external loading $\sigma_r(\theta) = \int_0^{2\pi} \sigma(\theta,\phi) d\phi$ exerted on this fraction [27] of the membrane by

$N_2 = -r^2\sigma_r(\theta) - N_1$ with

$$N_1 = \int_0^\theta r^2\sigma_r(\bar{\theta})\sin\bar{\theta}\cos\bar{\theta}\,d\bar{\theta}\,. \qquad (6)$$

Because the membrane thickness h is small compared to the cell radius r, we neglect area compressibility and obtain the relative membrane strain $\varepsilon_2 = \Delta r / r$ along the line trap ($\theta = \pi/2$) for small radial deformations Δr as

$$\varepsilon_2 = (N_2 - \nu N_1)/Eh\,, \qquad (7)$$

with Poisson coefficient $\nu = 0.5$ for biological membranes.

Figure 4 shows the stretching of RBCs measured at two different NA_x's, where a linear dependency on laser power is readily apparent. In experiments at NA_x = 0.39, close to the theoretical optimum range of NA_x = 0.45 – 0.6 (see Fig. 3), considerably larger elongation is observed than at lower NA_x = 0.28. Fitting the deformation calculated following Eq. (7) to our experimental results with the product of shear modulus and membrane thickness as a free parameter, best agreement is found at a value of $Gh = 5.8\cdot10^{-6}$ Nm^{-1}, where $Gh = Eh/2(1+\nu)$. This result compares well and falls within the scope of available literature values in the range of $3.7\cdot10^{-6}$ Nm^{-1} [6] to $7.5\cdot10^{-6}$ Nm^{-1} [24].

V. CONCLUSIONS

In this work, we investigate a new optical trapping method with inherent opposing forces that can be used to capture and stretch soft dielectric objects such as RBCs within a single line-shaped optical trap. As the astigmatic beam from a laser diode bar is focused

on the cell membrane, its refraction generates significant normal surface forces due to the inherent anisotropy of the beam's intensity distribution. As a result, directed antipodal elongation occurs along the linear trap within the ravine-like, optical potential landscape. Simulations modeling the beam paths of refracted rays illustrate the underlying stretching mechanism and are validated by our experimentally measured deformations.

As demonstrated in both our force calculations and experimental results, cell elongation occurs along the length of the linear trap, orthogonal to the axis of beam propagation. This is a significant result as it allows alignment of the major deformation axis with fluid flow streamlines, liberating optical stretching from the need to overcome forces due to viscous drag that prevent increasing throughput [12]. This ability to measure cell deformation in flowing environments makes throughput limited only by cell relaxation, increasing potential measurement rates several orders of magnitude. In addition, the same optical system can now be used for sample manipulation and observation. As a result, there is no need to integrate laser light perpendicular to the optical path [8] or to employ or align multiple beams [9], thus greatly simplifying application.

The significant additional benefit we identify via force modeling and the determination of optimal system parameters is that maximized stretching efficiency is observed with lower *NA* optical systems. This unique feature associated with the particular nature of linear laser traps greatly facilitates implementation for potential applications using inexpensive laser sources and simple optics. Additionally, the high

stretching efficiency allows minimization of required laser powers and any potential associated cell damage.

We acknowledge support from the National Science Foundation grant # DBI-0852868 and the National Institutes of Health under grant 1R01 AI079347.

[1] A. Ashkin, J. M. Dziedzic, J. E. Bjorkholm and S. Chu, Opt. Lett. **11,** 288 (1986).

[2] A. Ashkin, J. M. Dziedzic and T. Yamane, Nature **330,** 769 (1987).

[3] S. Suresh, J. Spatz, J. P. Mills, A. Micoulet, M. Dao, C. T. Lim, M. Beil and T. Seufferlein, Acta. Biomater. **1,** 15 (2005).

[4] S. Suresh, J. Mater. Res. **21,** 1871 (2006).

[5] S. Henon, G. Lenormand, A. Richert and F. Gallet, Biophys. J. **76,** 1145 (1999).

[6] M. Dao, C. T. Lim and S. Suresh, J. Mech. Phys. Solids **53,** 493 (2005).

[7] J. Guck, R. Ananthakrishnan, H. Mahmood, T. J. Moon, C. C. Cunningham and J. Käs, Biophys. J. **81,** 767 (2001).

[8] J. Guck, R. Ananthakrishnan, T. J. Moon, C. C. Cunningham and J. Käs, Phys. Rev. Lett. **84,** 5451 (2000).

[9] G. B. Liao, P. B. Bareil, Y. L. Sheng and A. Chiou, Opt. Express **16,** 1996 (2008).

[10] S. Rancourt-Grenier, M. T. Wei, J. J. Bai, A. Chiou, P. P. Bareil, P. L. Duval and Y. L. Sheng, Opt. Express **18,** 10462 (2010).

[11] T. Kaneta, J. Makihara and T. Imasaka, Anal. Chem. **73,** 5791 (2001).

[12] B. Lincoln, S. Schinkinger, K. Travis, F. Wottawah, S. Ebert, F. Sauer and J. Guck, Biomed. Microdevices **9,** 703 (2007).

[13] I. Sraj, C. D. Eggleton, R. Jimenez, E. Hoover, J. Squier, J. Chichester and D. W. M. Marr, J. Biomed. Opt. **15,** 047010 (2010).

[14] I. Sraj, A. C. Szatmary, S. A. Desai, D. W. M. Marr and C. D. Eggleton, Phys. Rev. E **85,** 041923 (2012).

[15] P. B. Bareil, Y. L. Sheng and A. Chiou, Opt. Express **14,** 12503 (2006).

[16] I. Sraj, A. C. Szatmary, D. W. M. Marr and C. D. Eggleton, Opt. Express **18,** 16702 (2010).

[17] T. Yu, F. C. Cheong and C. H. Sow, Nanotechnology **15,** 1732 (2004).

[18] P. L. Biancaniello and J. C. Crocker, Rev Sci Instrum **77,** 113702 (2006).

[19] R. W. Applegate, J. Squier, T. Vestad, J. Oakey and D. W. M. Marr, Opt. Express **12,** 4390 (2004).

[20] R. W. Applegate, J. Squier, T. Vestad, J. Oakey, D. W. M. Marr, P. Bado, M. A. Dugan and A. A. Said, Lab on a Chip **6,** 422 (2006).

[21] R. W. Applegate, D. W. M. Marr, J. Squier and S. W. Graves, Opt. Express **17,** 16731 (2009).

[22] E. A. Evans and R. M. Hochmuth, Biophys. J. **16,** 1 (1976).

[23] R. M. Hochmuth, P. R. Worthy and E. A. Evans, Biophys. J. **26,** 101 (1979).

[24] R. M. Hochmuth, J. Biomech. Eng.-T. ASME **115,** 515 (1993).

[25] Y. Park, C. A. Best, K. Badizadegan, R. R. Dasari, M. S. Feld, T. Kuriabova, M. L. Henle, A. J. Levine and G. Popescu, PNAS **107,** 6731 (2010).

[26] Y. N. Xia and G. M. Whitesides, Annu. Rev. Mater. Sci. **28,** 153 (1998).

[27] E. Ventsel and T. Krauthammer, *Thin Plates and Shells: Theory, Analysis, and Applications* (Marcel Dekker, New York, 2001).

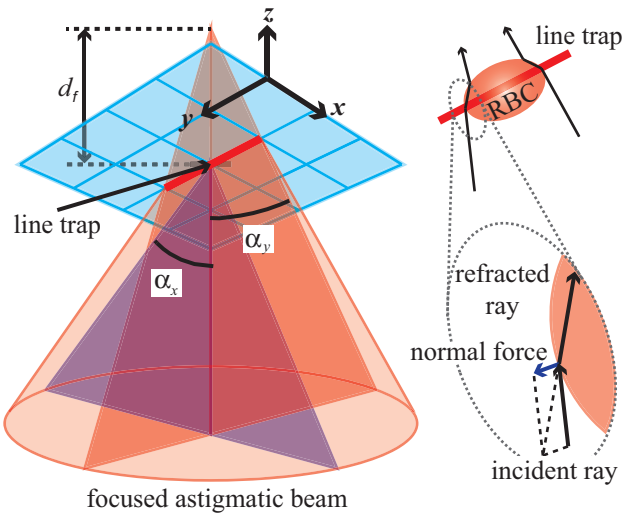

FIG. 1 (color online). An astigmatic laser beam is focused, creating a line-shaped optical trap due to the different focal planes of its axes. A RBC is stretched within the resulting optical potential, deforming in the transverse beam direction via transferred momenta normal to the cell surface.

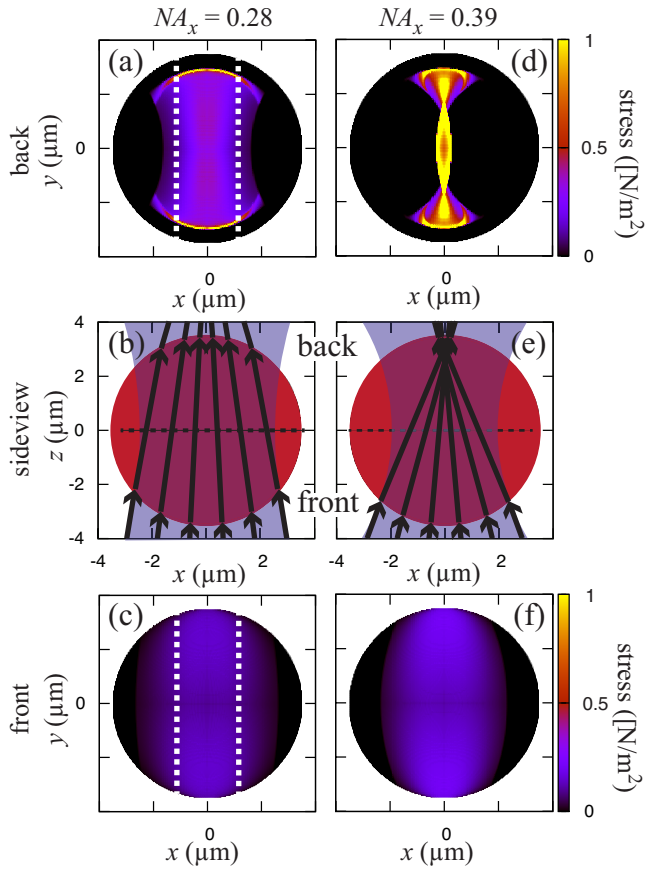

FIG. 2 (color online). Contour plots show the stress distribution over the cell membrane on the back (a) and front side (c) in the direction of the incident beam for $NA_x = 0.28$ where dotted lines indicate the direction of the linear trap. (d) and (f) show both sides for $NA_x = 0.39$. Side views (b) and (e) illustrate the light of a focused Gaussian beam refracted by a cell trapped in the focal plane $z = 0$, indicating the influence of incident light NA_x.

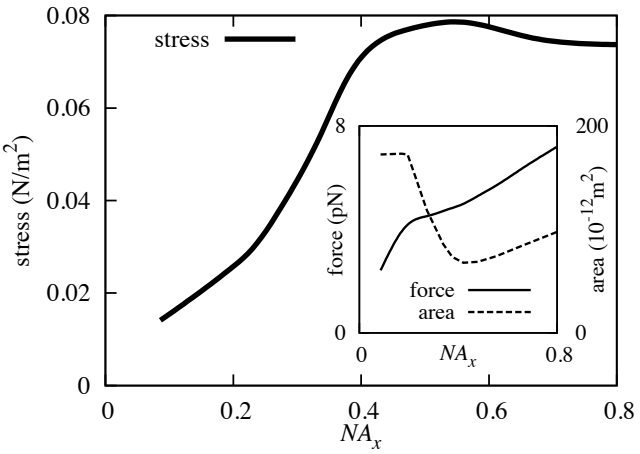

FIG. 3. Membrane stress generated over the surface of a typically sized RBC along the linear trap varies with the NA_x of the focused laser beam. The inset shows the stretching forces increasing with NA_x (solid), while the cell surface area exposed to laser light (dashed) exhibits a clear minimum. Note here the relatively low NA_x at which the maximum stretching efficiency occurs.

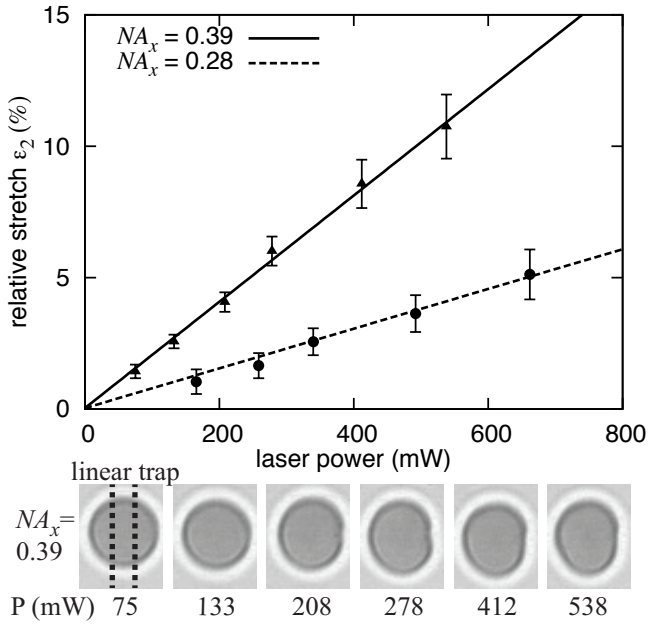

FIG. 4. Measured relative elongation of RBCs vs. applied laser power and focusing objective NA_x, where a significantly different stretching efficiency with laser power can be seen. Observed deformations agree well with simulation data shown as solid and dashed lines.